Article

Polynuclear Cation#Cation Complexes of Pentavalent Uranyl: Relating Stability and Magnetic Properties to Structure

Gre#gory Nocton, Pawel Horeglad, Jacques Pe#caut, and Marinella Mazzanti

J. Am. Chem. Soc., **2008**, 130 (49), 16633-16645 • DOI: 10.1021/ja804766r • Publication Date (Web): 17 November 2008

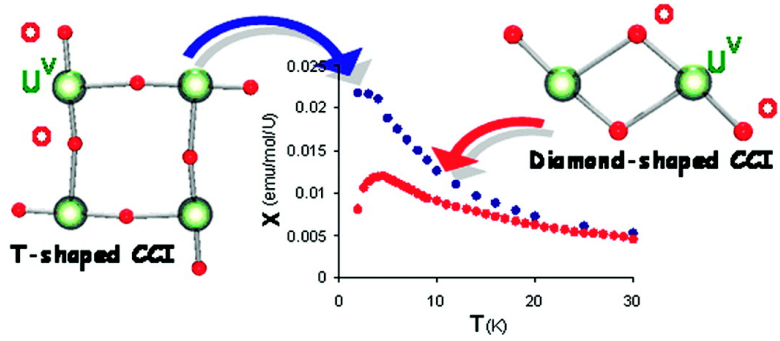

More About This Article

Additional resources and features associated with this article are available within the HTML version:

- Supporting Information
- Access to high resolution figures
- Links to articles and content related to this article
- Copyright permission to reproduce figures and/or text from this article

View the Full Text HTML

J|A|C|S
ARTICLES

Published on Web 11/17/2008

Polynuclear Cation−Cation Complexes of Pentavalent Uranyl: Relating Stability and Magnetic Properties to Structure

Grégory Nocton, Pawel Horeglad, Jacques Pécaut, and Marinella Mazzanti*

Laboratoire de Reconnaissance Ionique et Chimie de Coordination, Service de Chimie Inorganique et Biologique (UMR-E 3 CEA-UJF), INAC, CEA-Grenoble, 38054 Grenoble Cedex 09, France

Received June 22, 2008; E-mail: marinella.mazzanti@cea.fr

Abstract: Reaction of $\{[UO_2Py_5][\mu\text{-}KI_2Py_2]\}_n$ (**1**) with 2 equiv of potassium dibenzoylmethanate (Kdbm) in pyridine or acetonitrile affords, respectively, the corresponding tetranuclear complexes of pentavalent uranyl $\{[UO_2(dbm)_2]_2[\mu\text{-}K(Py)_2]_2[\mu_8\text{-}K(Py)]\}_2I_2\cdot Py_2$ (**2**) (in 70% yield) and $\{[UO_2(dbm)_2]_2[\mu\text{-}K(MeCN)_2][\mu_8\text{-}K]\}_2$ (**3**) (in 40% yield) in which four UO_2^+ are mutually coordinated (T-shaped "cation−cation" interaction). The X-ray structures of **2** and **3** show also the presence of, respectively, six and four potassium cations involved in $UO_2^+\cdots K^+$ interactions. Reaction of **2** with an excess of 18-crown-6 (18C6) affords the dimeric complex $[UO_2(dbm)_2K(18C6)]_2$ (**4**) presenting a diamond-shaped interaction between two UO_2^+ groups, in 45% yield. ^{1}H and PFGSTE diffusion NMR spectroscopy of **2** and **3** in pyridine show unambiguously the presence of $UO_2^+\cdots UO_2^+$ and $UO_2^+\cdots K^+$ interactions (tetrametallic species) in solution, which leads to a rapid (7 days) disproportionation of pentavalent uranyl to afford $[U(dbm)_4]$ and $[UO_2(dbm)_2]$ species. The $UO_2^+\cdots K^+$ interaction plays an important synergistic role in the stabilization of the $UO_2^+\cdots UO_2^+$ interactions. Accordingly, the lower affinity of $(K(18C6))^+$ for the uranyl(V) oxygen in complex **4** results in a lower number of coordinated K^+ and therefore in a weakened $UO_2^+\cdots UO_2^+$ interaction. The $UO_2^+\cdots UO_2^+$ interactions is completely disrupted in dmso or in the presence of Kdbm, preventing disproportionation of pentavalent uranyl. Solid-state variable-temperature magnetic susceptibility studies showed the unambiguous presence of antiferromagnetic coupling between the two oxo-bridged uranium centers of complex **4**, with the appearance of a maximum in χ versus T at ∼5 K. The different behavior of the tetrameric complex **3**, which probably involves a magnetic coupling occurring at lower temperature, can be ascribed to the different geometric arrangement of the interacting uranyl(V) groups.

Introduction

The chemistry of actinyl cations ($AnO_2^{+/2+}$) plays a crucial role both in nuclear technology and in the environmental mobility of actinides.[1,2] In particular, the mutual coordination of one actinyl oxo atom as an equatorial ligand to the actinide center of an adjacent group, also known as a "cation−cation" interaction[3] (CCI), plays a key role in the solid-state and solution chemistry of these species. While the oxo groups of the uranyl(VI) cation (UO_2^{2+}) are rarely involved in the coordination of other cations,[4−6] CCIs are frequently found in the solid-state structures of (NpO_2^+),[7] probably as a result of the higher negative charge of the oxo groups in the pentavalent neptunyl. CCIs play a critical role in the enhancement of magnetic interactions between neptunium ions, giving rise to ferromagnetic (or more rarely to antiferromagnetic) ordering through a superexchange pathway.[8−10] CCIs have also been reported to play an important role in the rapid aqueous disproportionation of pentavalent uranyl UO_2^+ to U(IV) and uranyl(VI) species.[11,12] Recent theoretical studies[13] suggest that the disproportionation proceeds via the formation of dimeric CCI complexes, but unambiguous experimental evidence for the presence of such species in solution and of their implication in the disproportionation is lacking.[14]

Except at low pH $(2-2.5)^2$ and in concentrated carbonate media, UO_2^+ is highly unstable in water.[15−17] However, pentavalent uranyl is an important intermediate in biomediated

(1) May, I.; Copping, R.; Cornet, S. M.; Talbot-Eeckelears, C. E.; Gaunt, A. J.; John, G. H.; Redmond, M. R.; Sharrad, C. A.; Sutton, A. D.; Collison, D.; Fox, O. D.; Jones, C. J.; Sarsfield, M. J.; Taylor, R. J. *J. Alloys Compd.* **2007**, *444*, 383–386.
(2) Edelstein, N. M.; Lander, G. H. *The Chemistry of the Actinide and Transactinide Elements*; Springer: Dordrecht, 2006.
(3) Sullivan, J. C.; Zielen, A. J.; Hindman, J. C. *J. Am. Chem. Soc.* **1961**, *83*, 3373–3378.
(4) Kubatko, K.-A.; Burns, P. C. *Inorg. Chem.* **2006**, *45*, 10277–10281.
(5) Sarsfield, M. J.; Helliwell, M. *J. Am. Chem. Soc.* **2004**, *126*, 1036–1037.
(6) Sullens, T. A.; Jensen, R. A.; Shvareva, T. Y.; Albrecht-Schmitt, T. E. *J. Am. Chem. Soc.* **2004**, *126*, 2676–2677.
(7) Krot, N. N.; Grigoriev, M. S. *Russ. Chem. Rev.* **2004**, *73*, 89–100.
(8) Forbes, T. Z.; Burns, P. C.; Soderholm, L.; Skanthakumar, S. *Chem. Mater.* **2006**, *18*, 1643–1649.
(9) Almond, P. M.; Skanthakumar, S.; Soderholm, L.; Burns, P. C. *Chem. Mater.* **2007**, *19*, 280–285.
(10) Forbes, T. Z.; Burns, P. C.; Skanthakumar, S.; Soderholm, L. *J. Am. Chem. Soc.* **2007**, *129*, 2760–2761.
(11) Ekstrom, A. *Inorg. Chem.* **1974**, *13*, 2237–2241.
(12) Newton, T. W.; Baker, F. B. *Inorg. Chem.* **1965**, *4*, 1166–1170.
(13) Steele, H.; Taylor, R. J. *Inorg. Chem.* **2007**, *46*, 6311–6318.
(14) Szabo, Z.; Toraishi, T.; Vallet, V.; Grenthe, I. *Coord. Chem. Rev.* **2006**, *250*, 784–815.
(15) Ikeda, A.; Hennig, C.; Tsushima, S.; Takao, K.; Ikeda, Y.; Scheinost, A. C.; Bernhard, G. *Inorg. Chem.* **2007**, *46*, 4212–4219.

reduction of stable hexavalent uranyl ions,[18,19] making its chemistry highly relevant for the understanding of uranium mobility in the environment and for the development of remediation strategies. Moreover, stable UO_2^+ complexes are ideal candidates for the development of photocatalysts and for active materials for efficient electric power storage due to the reversibility of the electron-transfer reaction $UO_2^{2+}\cdots UO_2^+$ and to the possibility of photochemically generating highly reducing UO_2^+ intermediates.[20,21] While spectroscopic studies of electrochemically prepared UO_2^+ compounds suggested higher stability of UO_2^+ in organic anhydrous media,[22,23] only recently have a few UO_2^+ complexes been isolated and crystallographically characterized.[24−27] Among these, the stable pyridine solvate of the pentavalent uranyl iodide $\{[UO_2Py_5][\mu\text{-}KI_2Py_2]\}_n$, **1**,[28] (**I**) is an excellent precursor for the study of the coordination chemistry of pentavalent uranyl.[29,30] Some of the isolated complexes show CCIs with alkali or transition metal cations, but no $UO_2^+\cdots UO_2^+$ interactions were demonstrated so far for any of these compounds in the solid state or in solution.

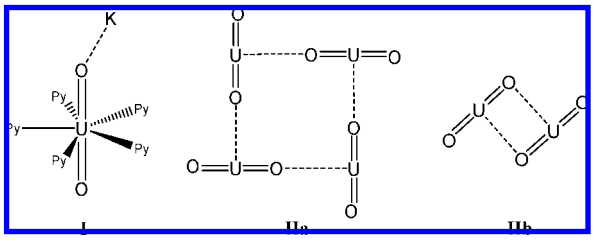

Beside the crucial information that the structural and reactivity studies of cation−cation complexes can provide in the understanding of the disproportionation mechanism and the development of new synthetic strategies for the preparation of solution stable UO_2^+ complexes, CCIs also provide a route to the assembly of multimetallic uranium complexes. The design of multimetallic molecular actinide complexes with magnetic exchange interactions between actinide centers is of high current interest as models for the understanding of the electronic structure of actinide materials and because they could lead to the development of actinide-based functional materials.[2,31,32] However, among the few reported polymetallic uranium complexes[33,34] for which the magnetic properties have been investigated, in only one case have unambiguous f^1-f^1 magnetic coupling between uranium centers been observed.[35] Notably in the dimeric U(V) imido complex $[(MeC_5H_4)_3U_2][\mu\text{-}1,4\text{-}N_2C_6H_4]$ antiferromagnetic coupling between the U(V) centers is mediated by the imido linkage.

We recently showed that the reaction of **1** with potassium dibenzoylmethanate (Kdbm) in pyridine allows isolation of crystals of the first example of a UO_2^+ complex having a T-shaped $UO_2^+\cdots UO_2^+$ interaction (**IIa**).[29] Here we describe the synthetic procedure allowing the isolation in a pure form of two new cation−cation complexes of dibenzoylmethanate (dbm^-) with different nuclearity presenting T-shaped (**IIa**) or diamond-shaped (**IIb**) (dinuclear) CCIs together with their structural characterization and stability studies under different conditions. Magnetic susceptibility measurements allow us to demonstrate the first unambiguous example of magnetic coupling between uranium centers mediated by an oxo group in molecules.

Results and Discussion

Synthesis, Crystal, and Molecular Structure. The polymeric pentavalent uranyl iodide $\{[UO_2Py_5][\mu\text{-}KI_2Py_2]\}_n$ (**1**) was prepared in 75% yield via the oxidation of U(III) with a mixture of water and PyNO followed by addition of potassium iodide.[28] Compound **1** reacts rapidly with O_2 or pyridine-*N*-oxide in pyridine to form the U(VI) adduct $[UO_2I_2(Py)_3]$, whereas the reaction with water proceeds more slowly (is completed after 1 week) and leads to unidentified products. Complex **1** is soluble in dmso and acetonitrile where it rapidly decomposes but is stable enough for coordination chemistry studies. A higher stability associated with a lower solubility is observed in pyridine and thf. Accordingly compound **1** is an excellent starting material for the development of the coordination chemistry of pentavalent uranyl in different solvents.[30]

The reaction of **1** with 2 equiv of Kdbm salt (dbm^- = dibenzoylmethanate) in pyridine or in acetonitrile leads to the respective solvate bis-ligand complexes in 75% (pyridine) and 40% (acetonitrile) yield (Scheme 1). The crystal structure of the pyridine solvate $\{[UO_2(dbm)_2]_2[\mu\text{-}K(Py)_2]_2[\mu_8\text{-}K(Py)]\}_2I_2\cdot Py_2$ (**2**) has been reported in a preliminary communication.[29] Crystals of the acetonitrile solvate $\{[UO_2(dbm)_2]_2[\mu\text{-}K(MeCN)_2][\mu_8\text{-}K]\}_2$ (**3**) were obtained by letting stand a concentrated (24 mM) solution of the complex **3** in acetonitrile at room temperature. The tetrameric UO_2^+ complexes of dbm^- can be isolated analytically pure from pyridine by diffusion of diisopropylether (over 1 h), while longer crystallization times in pyridine can result in contamination by disproportionation products. Complex **2** slowly disproportionates in pyridine solution to form the $[U^{IV}(dbm)_4]$ and $[U^{VI}O_2(dbm)_2]$ complexes. However, the time scale of the disproportionation (hours) allows the isolation and characterization of **2** by NMR. The disproportionation occurs

(16) Docrat, T. I.; Mosselmans, J. F. W.; Charnock, J. M.; Whiteley, M. W.; Collison, D.; Livens, F. R.; Jones, C.; Edmiston, M. J. *Inorg. Chem.* **1999**, *38*, 1879–1882.
(17) Clark, D. L.; Hobart, D. E.; Neu, M. P. *Chem. Rev.* **1995**, *95*, 25–48.
(18) Ilton, E. S.; Haiduc, A.; Cahill, C. L.; Felmy, A. R. *Inorg. Chem.* **2005**, *44*, 2986–2988.
(19) Renshaw, J. C.; Butchins, L. J. C.; Livens, F. R.; May, I.; Charnock, J. M.; Lloyd, J. R. *Environ. Sci. Technol.* **2005**, *39*, 5657–5660.
(20) Shirasaki, K.; Yamamura, T.; Shiokawa, Y. *J. Alloys Compd.* **2006**, *408*, 1296–1301.
(21) Bakac, A.; Espenson, J. H. *Inorg. Chem.* **1995**, *34*, 1730–1735.
(22) Mizuoka, K.; Tsushima, S.; Hasegawa, M.; Hoshi, T.; Ikeda, Y. *Inorg. Chem.* **2005**, *44*, 6211–6218.
(23) Kim, S. Y.; Asakura, T.; Morita, Y.; Uchiyama, G.; Ikeda, Y. *Radiochim. Acta* **2005**, *93*, 75–81.
(24) Berthet, J.-C.; Nierlich, M.; Ephritikhine, M. *Angew. Chem., Int. Ed.* **2003**, *42*, 1952–1954.
(25) Berthet, J. C.; Siffredi, G.; Thuery, P.; Ephritikhine, M. *Chem. Commun.* **2006**, 3184–3186.
(26) Hayton, T. W.; Wu, G. *J. Am. Chem. Soc.* **2008**, *130*, 2005–2014.
(27) Arnold, P. L.; Patel, D.; Wilson, C.; Love, J. B. *Nature* **2008**, *451*, 315–U313.
(28) Natrajan, L.; Burdet, F.; Pecaut, J.; Mazzanti, M. *J. Am. Chem. Soc.* **2006**, *128*, 7152–7153.
(29) Burdet, F.; Pecaut, J.; Mazzanti, M. *J. Am. Chem. Soc.* **2006**, *128*, 16512–16513.
(30) Horeglad, P.; Nocton, G.; Pécaut, J.; Mazzanti, M. Manuscript in preparation.
(31) Schelter, E. J.; Wu, R. L.; Scott, B. L.; Thompson, J. D.; Morris, D. E.; Kiplinger, J. L. *Angew. Chem., Int. Ed.* **2008**, *47*, 2993–2996.
(32) Curro, N. J.; Caldwell, T.; Bauer, E. D.; Morales, L. A.; Graf, M. J.; Bang, Y.; Balatsky, A. V.; Thompson, J. D.; Sarrao, J. L. *Nature* **2005**, *434*, 622–625.
(33) Ephritikhine, M. *Dalton Trans.* **2006**, 2501–2516.
(34) Evans, W. J.; Kozimor, S. A.; Ziller, J. W. *Science* **2005**, *309*, 1835–1838.
(35) Rosen, R. K.; Andersen, R. A.; Edelstein, N. M. *J. Am. Chem. Soc.* **1990**, *112*, 4588–4590.

Scheme 1

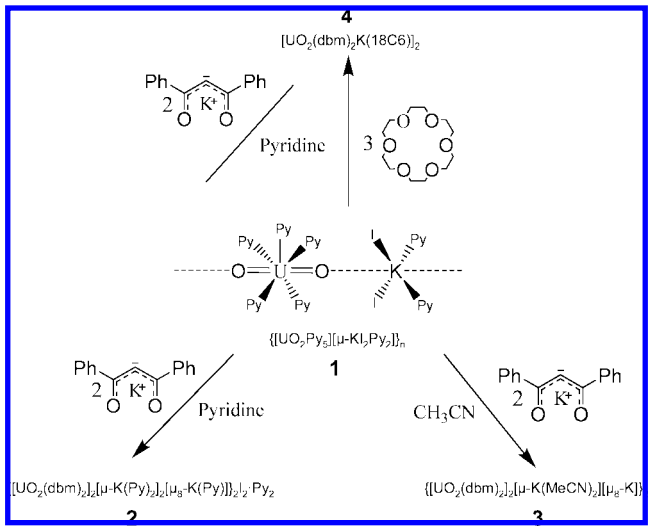

faster in acetonitrile, but the lower solubility of **3** with respect to the U(IV) and $U^{VI}O_2^{2+}$ species allows the isolation of **3** in a pure form in relatively high yield.

ORTEP views of the cation $\{[UO_2(dbm)_2]_2[\mu\text{-}K(Py)_2]_2[\mu_8\text{-}K(Py)\}^{2+}$ in **2**[29] and of **3** are presented in Figures 1−3 together with schematic representations of the structure, and selected bond distances and angles are given in Table 1. Structures of both **2** and **3** consist of centrosymmetric tetramers where two inequivalent uranyl(V) groups are coordinated to each other in a monodentate fashion to form a square plane. In both structures each UO_2^+ coordinates two adjacent uranyl(V) groups resulting in a T-shaped CCI (two UO_2^+ groups arranged perpendicular to each other).

In **2** and **3** each UO_2^+ is also coordinated by the four oxygens of two bidentate dbm^- ligands resulting in the presence of four seven-coordinate uranium ions with a pentagonal bipyramidal geometry with uranyl(V) oxygen atoms in the axial positions. The main difference between the structures of **2** and **3** is the number of potassium ions involved in an additional CCI with the UO_2^+ oxygens. In **2** eight uranyl(V) oxygens interact with six potassium (three crystallographically inequivalent) ions arranged in an octahedral fashion around the plane formed by the four uranyl(V) ions with four potassium ions forming a square plane that includes the plane of the uranyl(V) ions and two potassium ions located below and above this plane (at 2.60 Å). The potassium ions K(1) and K(3), in the plane, are coordinated by two bridging dbm^- oxygens, one uranyl(V) oxygen, and two pyridine nitrogens. Another uranyl(V) oxygen from an adjacent $[UO_2(dbm)_2]^-$ complex is located at a longer distance (3.613 and 3.10(1) Å for K(1) and K(3), respectively). The two potassium ions in apical positions are nine-coordinated by four bridging dbm^- oxygens connecting four different uranyl(V) complexes, by four uranyl(V) oxygens, and by one pyridine nitrogen. In **3**, only four bridging potassium ions (two crystallographically inequivalent) are involved in a CCI with the uranyl(V) oxygens resulting in a neutral molecule, whereas in the structure of complex **2** two iodide anions balance the charge due to the additional potassium ions. In **3**, only two crystallographically equivalent potassium ions are found in the plane formed by the four interacting uranyl(V) groups. The coordination environment of the potassium ions is very similar in the two structures, beside the absence of solvent coordinated to the apical potassium ion in **3**. In both complexes shorter K−O (2.58(1)−2.68(1) Å) bond distances are found for potassium ions binding uranyl(V) oxygens not involved in CCI as compared to those found for potassium ions binding uranyl(V) oxygens involved in a CCI (3.10(1)−3.39(1) Å). In both complexes the identity of the UO_2^+ groups is not lost in the formation of the cation−cation complex; however, the CCIs result nevertheless in a significant lengthening of the involved U═O bonds (1.916(10) −1.924(9) Å), while the value of the $U-O_{yl}$ distances (1.808(10) and 1.830(10) Å) for the oxo groups not involved in $UO_2^+\cdots UO_2^+$ interactions are similar to those found in complex **1** (1.836(2) and 1.834(2) Å)[28] and in the two other reported mononuclear pentavalent uranyl complexes (ranging from 1.810(4) to 1.828(4) Å).[24,26] This desymmetrization, which results in a mean difference between the two U═O bonds of 0.11 Å, is the consequence of the strong electrostatic interaction between the two UO_2^+ cations. A similar desymmetrization of the uranyl(V) fragment has also been recently observed in dinuclear complexes presenting a $UO_2^+\cdots M^{2+}$ (M = Fe, Zn) interaction.[27]

Table 1. Selected Structural Parameters for **2** and **3** (#1 = $-x+1, -y+2, -z+1$ for **2** and #1 = $-x+3/2, -y+3/2, -z$ for **3**; Distances in Å, Angles in deg)

structural parameters	2	3
U(1)−O(14)	1.830(10)	1.808(10)
U(1)−O(11)	1.924(10)	1.916(10)
U(1)−O(13)#1	2.346(8)	2.400(9)
mean $U(1)-O_{dbm}$	2.45(1)	2.45(2)
U(2)−O(13)	1.934(8)	1.924(9)
U(2)−O(12)	1.812(9)	1.830(10)
U(2)−O(11)	2.37(1)	2.41(1)
mean $U(2)-O_{dbm}$	2.43(2)	2.44(4)
K(1)−O(12)	2.58(1)	2.59(1)
K(1)−O(11)	3.613(1)	3.39(1)
mean $K(1)-O_{dbm}$	2.9(3)	2.9(2)
$K(1)-N_{Py\ orACN}$	2.86(0)	2.82(2)
Mean $K(2)-O_{dbm}$	2.82(6)	2.78(3)
$K(2)-N_{py}$	2.905(15)	
mean $K(2)-O_{yl}$	3.32(9)	3.04(10)
K(3)−O(14)#1	2.68(1)	
K(3)−O(13)	3.10(1)	
mean $K(3)-O_{dbm}$	2.8(1)	
$K(3)-N_{py}$	2.88(2)	
mean U−U	4.278(6)	4.318(6)
O(14)−U(1)−O(11)	179.0(4)	179.3(5)
O(14)−U(1)−O(13)#1	90.7(4)	95.8(4)
O(11)−U(1)−O(13)#1	88.4(3)	84.8(4)
O(12)−U(2)−O(13)	178.9(4)	177.2(5)
O(12)−U(2)−O(11)	92.1(4)	92.0(4)
O(13)−U(2)−O(11)	88.5(3)	85.4(4)
U(1)−O(13)−U(2#1)	173.8(5)	171.6(5)

The difference in the number of potassium ions coordinated to the UO_2^+ oxygens in **2** and **3** leads only to some small but significant modification of the metric parameters in the square plane defined by the $UO_2^+\cdots UO_2^+$ interaction as highlighted in Figure 4. The main difference in the structural parameters is the longer distance between the uranyl(V) oxygens and the uranium centers of the interacting UO_2^+ groups in complex **3** (2.400(9) Å) with respect to complex **2** (2.346(8) Å), which suggest the presence of a weaker $UO_2^+\cdots UO_2^+$ interaction in **3**, underlying the important role that the presence of coordinating cations can play in the stabilization of these interactions. Moreover shorter average $K(2)-O_{yl}$ (O_{yl} = uranyl(V) oxygen) distances are found in **3** (3.04(10) Å) with respect to **2** (3.32(9) Å); this indicates that the removal of two potassium ions is somewhat compensated for by a stronger K−O interaction of the remaining potassium ions.

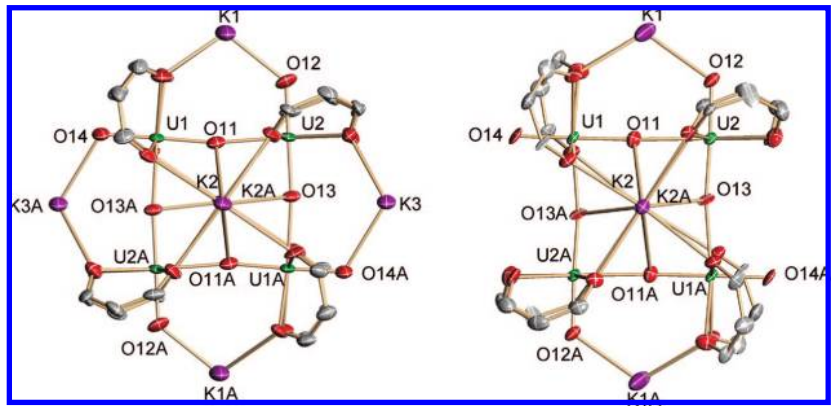

Figure 1. ORTEP views of the cation $\{[UO_2(dbm)_2]_2[\mu\text{-}K(Py)_2]_2[\mu_8\text{-}K(Py)]\}^{2+}$ of (left) **2** and (right) **3**. The structures are represented along the axis formed by the two potassium ions that are in apical positions with respect to the plane of the uranium atoms (H, the carbons of the phenyl groups of dbm^- ligands and all coordinated solvents molecules were omitted for clarity, thermal ellipsoid are at 30% level, C atoms are represented in gray, O in red, K in purple and U in green). (Symmetry transformations used to generate equivalent atoms $A = -x + 1, -y + 2, -z + 1$ for **2** and $A = -x + 3/2, -y + 3/2, -z$ for **3**.)

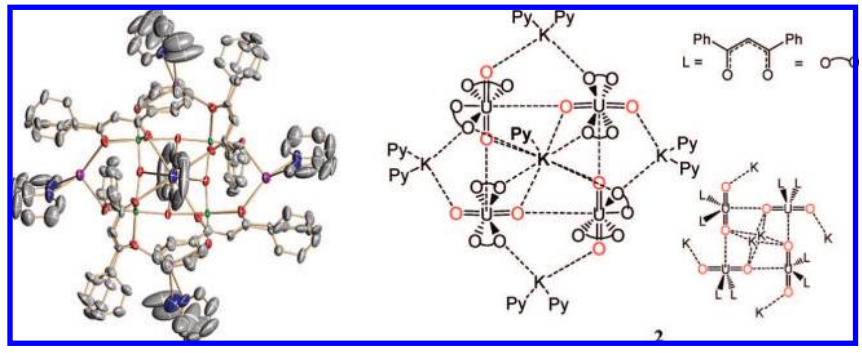

Figure 2. ORTEP view of **2** (left) and schematic representations of the structure (right). In the ORTEP view the structure is represented along the axis formed by the two potassium ions that are in apical positions with respect to the plane of the uranium atoms (H were omitted for clarity, thermal ellipsoid are at 30% level, C atoms are represented in gray, O in red, K in purple, N in blue and U in green).

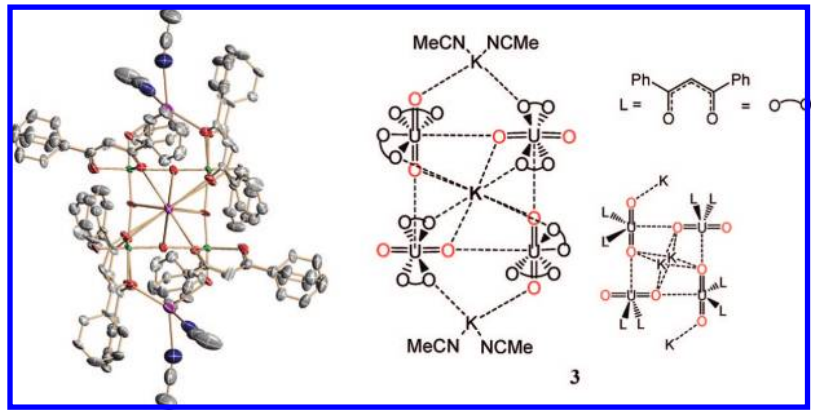

Figure 3. ORTEP view of **3** (left) and schematic representation of the structure (right). In the ORTEP view the structure is represented along the axis formed by the two potassium ions that are in apical positions with respect to the plane of the uranium atoms (H were omitted for clarity, thermal ellipsoid are at 30% level, C atoms are represented in gray, O in red, K in purple, N in blue, and U in green).

The coordination of the potassium counterions to the UO_2^+ oxygens in the tetrameric solid-state structures of **2** and **3** could play an important electronic or/and structural role in promoting the CCI in solution and therefore could influence the stability toward disproportionation. In order to evaluate these effects we have investigated the reaction of **2** with 18-crown-6 (18C6). We have taken advantage of the affinity of (18C6) for potassium to remove potassium from the structure and to reduce the acidity of eventual remaining bound potassium cations. The addition of 3 equiv of (18C6) to a 2:1 reaction mixture of Kdbm and **1** in pyridine resulted in a rapid color change from blue to green and analytically pure $[UO_2(dbm)_2K(18C6)]_2$, **4** was isolated in 45% yield in thf. Crystals of **4** suitable for X-ray diffraction were grown from a pyridine/hexane solution. **4** was found to crystallize as a centrosymmetric dimer in which two $[UO_2(dbm)_2]^-$ units are assembled through a diamond shaped CCIs (U−O−U angle = 101.7°) consisting of two mutually coordinated monodentate UO_2^+ groups. To our knowledge, only one example of this type of dimeric CCI has been previously ascribed to a NpO_2^+ complex.[7] The complex formula and the

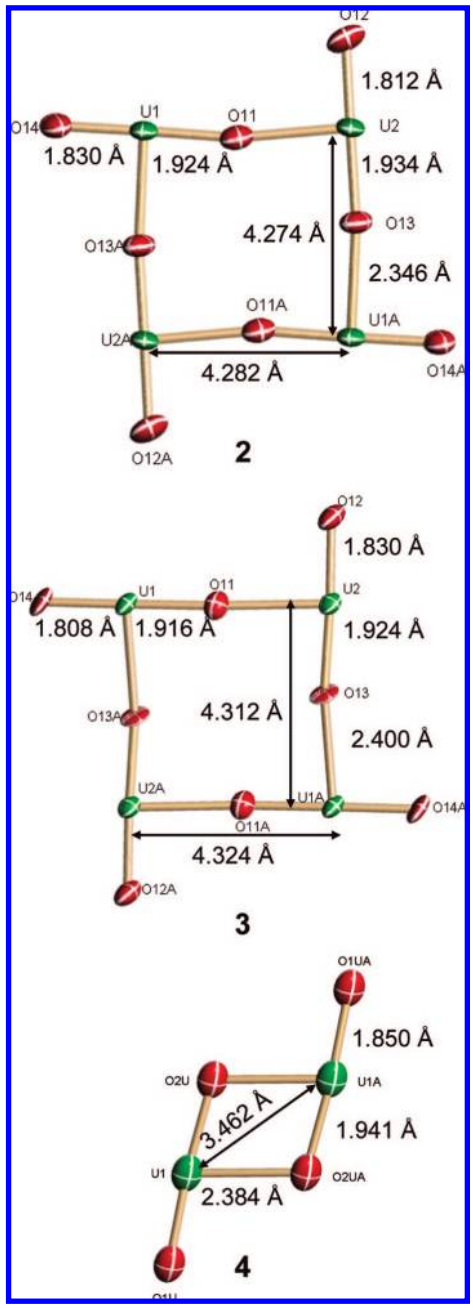

Figure 4. Details of the solid-state structures of **2**, **3**, and **4** showing the interacting $UO_2^+\cdots UO_2^+$ with associated distances (thermal ellipsoid are at 30% level, 20x atoms are represented in red and U atoms in green).

value of the U═O distances (1.941(4) and 1.850(4) Å) are in agreement with the presence of two pentavalent uranyl complexes. The structure of $[UO_2(dbm)_2K(18C6)]_2$ is shown in Figure 5.

Each UO_2^+ is also involved in a CCI with a (18C6) bound potassium ion through the uranyl(V) oxygen not involved in the $UO_2^+\cdots UO_2^+$ interaction. The value of the U═O−K distance of 2.760(5) Å falls in the range of U═O−K distances (2.658(6)−3.230(6) Å) reported for complexes of hexavalent uranyl forming a CCIs with an $[K(18C6)]^+$[36] and is significantly longer than the shorter U═O−K distance (2.58 Å) found in the tetramers **2** and **3**. The latter suggests that the interaction of the $[K(18C6)]^+$ cation with the pentavalent uranyl oxygen is significantly weaker than the one of K^+ alone. The U atoms in **4** are seven-coordinate, by two trans oxo groups in axial

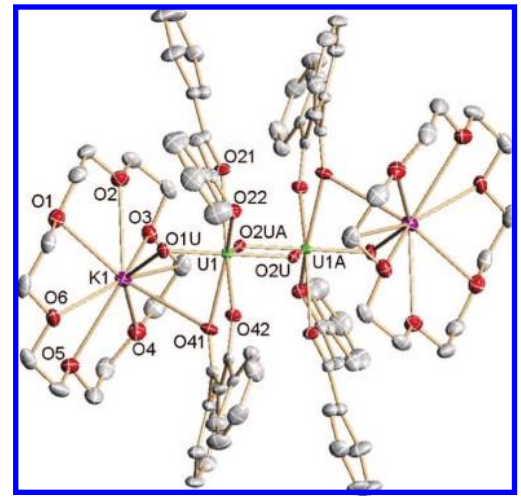

Figure 5. ORTEP view of $[UO_2(dbm)_2K(18C6)]_2$ (**4**) (thermal ellipsoid are at 30% level, C are represented in gray, O in red, K in purple, and U in green) Selected distances (Å) and angles (deg): U(1)−O(1U), 1.850(4); U(1)−O(2U), 1.941(4); U(1)−(2U)A, 2.384(4); U(1)−O(22), 2.410(4); U(1)−O(42), 2.422(4); U(1)−O(41), 2.435(4); U(1)−O(21), 2.442(4); O(1U)−K(1), 2.760(5); O(41)−K(1), 3.125(5); mean K−O18−C-6, 2.93(5); O(1U)−U(1)−O(2U), 175.80(18); O(1U)−U(1)−O(2U)A, 101.68(16); U(1)−O(1)−K(1), 110.11(18). (Symmetry transformations used to generate equivalent atoms A: $-x$, $-y$, $-z$).

positions, four oxygen atoms of two bidentate dbm^- ligands, and one bridging oxo group of the adjacent UO_2^+ in the equatorial plane. The dimeric structure results in a significant distortion of the coordination geometry from the ideal pentagonal bipyramidal geometry with the bridging oxo ligands located 0.995 Å below the mean plane formed by the other equatorial ligands. Similarly to what is observed in complexes **2** and **3**, the CCI in the case of **4** results in a desymmetrization of the UO_2^+ groups with a long (1.941(4) Å) and a shorter (1.850(4) Å) U−O distance. The U−O bond for the uranyl(V) oxygen coordinated to potassium (1.850(4) Å) is slightly longer with respect to monomeric complexes reported in the literature (U−O distances in the range = 1.810(4)−1.828(4) Å)[24,26] that do not present binding cations, despite the weak coordinating ability of $[K(18C6)]^+$. The difference between the two U═O bonds is smaller (0.09 Å) than one observed in the tetramers **2** and **3** (0.11 Å), suggesting a weaker $UO_2^+\cdots UO_2^+$ interaction in the dimeric structure. However the difference remains much larger than the average difference observed in cation−cation complexes of pentavalent neptunium (0.04 Å), suggesting that even in this geometry a stronger interaction occurs in the uranium species.

Solution Structure. Although CCIs have been well characterized in the solid state for neptunyl(V) compounds, detailed solution-phase structural data have proved elusive despite the numerous studies that have used IR,[37] UV−vis,[38] Raman,[37] EXAFS,[38] or HEXS[39] spectroscopies. In this work we used for the first time NMR spectroscopy to unambiguously verify the presence of CCIs in solution.

The solution structure of the complexes **2**, **3**, and **4** in different solvent conditions was studied by UV−vis, ESI-MS, and 1-D

(36) Thuery, P.; Masci, B.; Takimoto, M.; Yamato, T. *Inorg. Chem. Commun.* **2007**, *10*, 795–799.
(37) Guillaume, B.; Begun, G. M.; Hahn, R. L. *Inorg. Chem.* **1982**, *21*, 1159–1166.
(38) Stout, B. E.; Choppin, G. R.; Nectoux, F.; Pages, M. *Radiochim. Acta* **1993**, *61*, 65–67.
(39) Skanthakumar, S.; Antonio, M. R.; Soderholm, L. *Inorg. Chem.* **2008**, *47*, 4591–4595.

Table 2. Diffusion Coefficient Measured at 400 MHz and 298 K, Calculated Hydrodynamic Radius, and Solution Molecular Weight for Complexes **2** (M = 4303.62 g mol^{-1}), **3** (M = 3391.91 g mol^{-1}), and **4** (M = 2039.34 g mol^{-1})

solvent	compound	D [m^2 s^{-1}]	r_{sph} [Å]	M_{sol} [g mol^{-1}] found	expected formula
dmso η = 1.987 mPa s (298 K)	$U^{VI}O_2(dbm)_2(dmso)$ (M = 794.7 g mol^{-1})	1.64(2) × 10^{-10}	6.7		
	2	1.56(3) × 10^{-10}	7.0	940 ± 75	$[UO_2(dbm)_2(dmso)]K$
pyridine η = 0.879 mPa s (298 K)	**2**	2.21(2) × 10^{-10}	11.3	4045 ± 250[a]	$\{[UO_2(dbm)_2]_4[\mu\text{-}K_6(Py)_x]\}^{2+}$
	$U^{IV}(dbm)_4$ (M = 1130 g mol^{-1})	3.52(3) × 10^{-10}	7.1		
	3	2.62(3) × 10^{-10}	9.5	2740 ± 260	$[UO_2(dbm)_2]_4[\mu\text{-}K_4(Py)_x]$
		3.68(3) × 10^{-10}	6.7	992 ± 80	$[UO_2(dbm)_2(Py)]K$
	4	3.65(5) × 10^{-10}[b]	6.8	1010 ± 110	$[UO_2(dbm)_2K(18C6)]$
pyridine/dmso 100:5	$U^{IV}(dbm)_4$ (M = 1130 g mol^{-1})	3.05(2) × 10^{-10}	[c]		
	2 A	2.13(9) × 10^{-10}	[c]	3317 ± 440	$\{[UO_2(dbm)_2]_4[\mu\text{-}K_6(Py)_x]\}^{2+}$
	2 B	2.32(2) × 10^{-10}	[c]	2567 ± 120	$[UO_2(dbm)_2]_4[\mu\text{-}K_4(Py)_x]$
	2 C	3.20(5) × 10^{-10}	[c]	978 ± 90	$[UO_2(dbm)_2(S)_x]K$

[a] Reference 29. [b] The molecular weight of K(18C6) (M = 303.2 g mol^{-1}) was found to be 678 g mol^{-1}. This indicates the presence of an exchange between free and uranyl(V) bound K(18C6). [c] The determination of r_{sph} was not possible because the information on the specific viscosity of the pyridine/dmso 100:5 mixture was not available. **A**, **B** and **C**: the dissolution of **2** in the Pyridine/dmso 100:5 mixture allowed us to measure the diffusion coefficient of three different sets of signals, which were respectively attributed to **2**, **3**, and the monomer $[UO_2(dbm)_2]K$. The calculated value of the spherical hydrodynamic radius (11.3 Å for **2** and 9.5 Å for **3** in pyridine) are in a good agreement with the value estimated from the crystal structure (10.8 Å for **2** and 10.0 for **3**).

and 2-D COSY, NOESY and PFGSTE diffusion NMR spectroscopy. All studies were performed immediately after dissolution of the isolated compounds to avoid the presence of the decomposition products which can be detected after few hours in pyridine or thf solution.

The translational diffusion coefficient (D) of the different species in pyridine and dmso was determined relative to a reference compound by NMR experiments (using a pulsed-field gradient stimulated echo (PFGSTE) sequence). Assuming that the studied species can be roughly modeled by spheres possessing a hydrodynamic radius r_{sph} ($r_{sph} = k_BT/6\pi\eta D$) where η (Pa s^{-1}) is the viscosity of the medium and k_B (m^2 kg^{-2} K^{-1}) is Boltzmann's constant. Their autodiffusion coefficients D are related to their molecular weight for compounds with similar partial specific volumes.[40] The determination of translational diffusion coefficients for shape-similar complexes is thus an efficient tool for deducing the molecular mass of unknown species in solution when a similar reference compound is measured under the same conditions (eq 1).[41] If an exchange process is occurring in the experiment time-scale between different solution species, only an average molecular weight can be obtained. The calculated values of spherical hydrodynamic radius and molecular weight with respect to a chosen reference of **2**, **3**, and **4** in pyridine solution and of **2** in dmso are presented in Table 2.

$$\frac{D_1}{D_2} = \sqrt[3]{\frac{M_2}{M_1}} \qquad (1)$$

The proton NMR spectrum of **2** in a 3.3 mM pyridine solution (Figure 6) recorded immediately after dissolution shows the presence of three sets of signals in the ratio 12:15:100 in agreement with the presence of one $C2v$ symmetric species and two rigid $C4h$ symmetric solution species.

The $C2v$ species were assigned by both 1-D and COSY NMR to a monomeric $[UO_2(dbm)_2(Py)]K$ complex. PFGSTE diffusion NMR experiments (after addition of 5% dmso) confirmed this assignment but do not demonstrate that the coordination of the potassium cation to the uranyl(V) oxygen occurs in this monomeric species. The two $C4h$ symmetric species were assigned, by 1-D and PFGSTE NMR experiments and by comparison of the spectrum of the isolated complex **3**, in pyridine solution, to the two T-shaped tetrameric assemblies $\{[UO_2(dbm)_2]_4[\mu\text{-}K_x(Py)_y]\}^{n+}$ ($x = 4$, $n = 0$ minor species and $x = 6$, $n = 2$ major species) containing a different number of potassium cations. The presence, in solution, of the tetrameric assembly was also confirmed by ESI-mass spectroscopy (ESI/MS m/z = 1549 $\{[UO_2(dbm)_2]_4K_6\}^{2+}$).

Dissolution of **2** in thf leads to a suspension. After filtration of the separated KI salt, the 1D NMR shows only the signals assigned to complex $[UO_2(dbm)_2]_4[\mu\text{-}K_4(thf)_x]$. Complex **3** once isolated is very insoluble in acetonitrile but soluble in pyridine and thf. The proton NMR spectrum of 1.6 mM thf solutions of complex **3** (Figure 7) recorded immediately after dissolution shows the presence of only one rigid $C4h$ symmetric solution species, in agreement with the presence in solution of the polymetallic assembly $[UO_2(dbm)_2]_4[\mu\text{-}K_4(thf)_x]$ and with the retention of the solid-state structure. A similar 1D NMR spectrum is observed when complex **3** is prepared in situ from the reaction of a 2:1 mixture of K(dbm) and **1** (12.8 mM) in CD_3CN (Figure S11, Supporting Information). The proton NMR spectrum of a 1.6 mM pyridine solution of **3** (Figure S12, Supporting Information) shows the presence of two sets of signals in the ratio 100:17, in agreement with the presence of the tetrameric $C4h$ symmetric solution species $[UO_2(dbm)_2]_4[\mu\text{-}K_4(Py)_x]$ and the monomeric $C2v$ symmetric species $[UO_2(dbm)_2(py)_x]K$. The NMR experiment do not demonstrate that the coordination of the potassium cation to the uranyl(V) oxygen occurs in the monomeric species. The assignment of these species was confirmed by PFGSTE diffusion NMR spectroscopy. These results show unambiguously that the $UO_2^+\cdots UO_2^+$ T-shaped interaction leading to a tetrameric assembly is retained completely in acetonitrile and thf, whereas the partial disruption of the tetrameric assembly to yield a monomeric species occurs in pyridine. Furthermore, the unambiguous presence of two different tetrameric solution species (corresponding to the isolated tetramers **2** and **3**) in pyridine shows that the $UO_2^+\cdots K^+$ cation−cation interaction is maintained in solution.

The evolution of the proton NMR spectrum after the addition of increasing amounts of dmso to a 3.4 mM pyridine solution of **2** (Figure S13, Supporting Information) shows an increase of the signals assigned to the tetrameric species $[UO_2(dbm)_2]_4[\mu\text{-}K_4(Py)_x]$ and of those assigned to the monomeric complex

(40) Waldeck, A. R.; Kuchel, P. W.; Lennon, A. J.; Chapman, B. E. *Prog. Nucl. Magn. Reson. Spectrosc.* **1997**, *30*, 39–68.
(41) Terazzi, E.; Torelli, S.; Bernardinelli, G.; Rivera, J. P.; Benech, J. M.; Bourgogne, C.; Donnio, B.; Guillon, D.; Imbert, D.; Bunzli, J. C. G.; Pinto, A.; Jeannerat, D.; Piguet, C. *J. Am. Chem. Soc.* **2005**, *127*, 888–903.

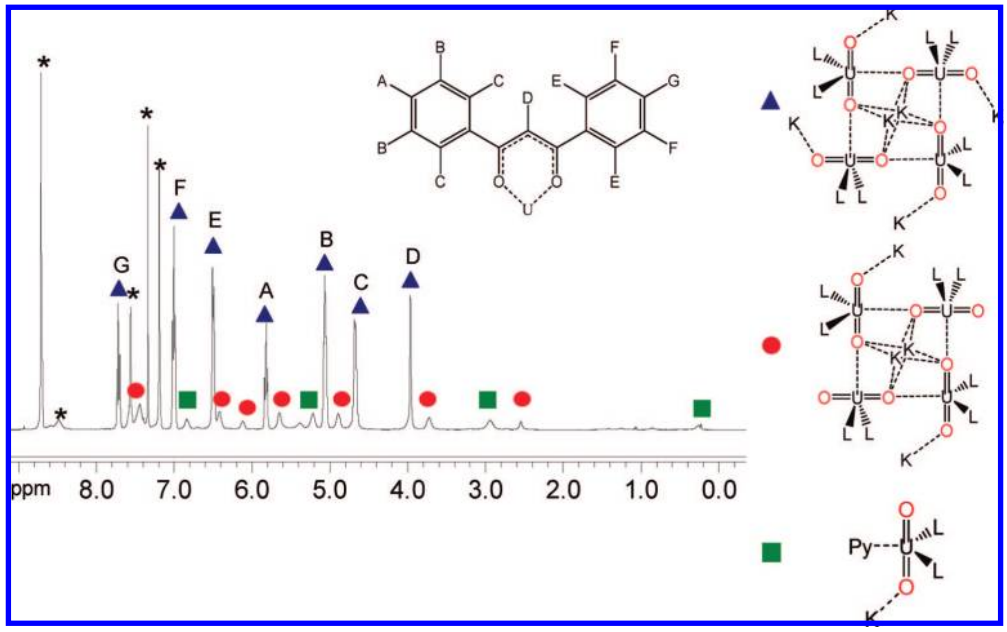

Figure 6. ^{1}H NMR spectrum at 400 MHz and at 298 K of a 3.3 mM solution of **2** in pyridine-d_5 solution. The seven signals of the major species $\{[UO_2(dbm)_2]_4[\mu\text{-}K_6(Py)_x]\}^{2+}$ are labeled with blue triangles (red dots label the signals assigned to $[UO_2(dbm)_2]_4[\mu\text{-}K_4(Py)_x]$ complex and green squares the signals assigned to the monomeric $[UO_2(dbm)_2(py)_x]K$ complex) (* = solvents and impurities).

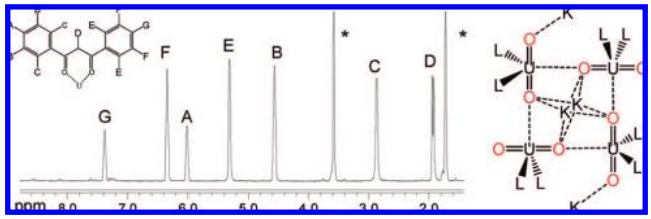

Figure 7. ^{1}H NMR spectrum at 400 MHz and at 298 K of **3** in thf-d_8 solution (1.6 mM) (* = thf).

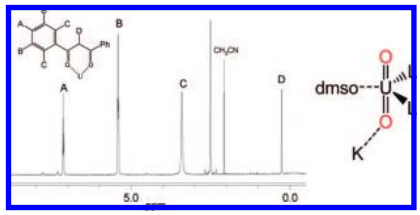

Figure 8. ^{1}H NMR spectrum at 400 MHz and 298 K of **3** (1.6 mM) in dmso-d_6.

accompanied by a decrease of the signals assigned to the tetrameric $\{[UO_2(dbm)_2]_4[\mu\text{-}K_6(Py)_x]\}^{2+}$ complex. These results show that the presence of increasing amounts of dmso, which can effectively compete with the uranyl(V) oxygens in the coordination of K^+ and UO_2^+, results in the disruption of the $K^+\cdots UO_2^+$ and of the $UO_2^+\cdots UO_2^+$ CCI to yield a monomeric species.

Solutions of **2** and **3** in deuterated dmso-d_6 show the same proton NMR spectra (Figure 8) with only one set of signals in agreement with the presence of the monomeric species $[UO_2(dbm)_2(dmso)_x]K$ in solution. The presence of the monomeric complex was confirmed by PFGSTE diffusion NMR performed on complex **3**, but do not demonstrate that the coordination of the potassium cation to the uranyl(V) oxygen occurs in this monomeric species. The strongly coordinating dmso ligand effectively competes with the uranyl(V) oxygen for the fifth coordination site at the uranyl(V) metal centers,

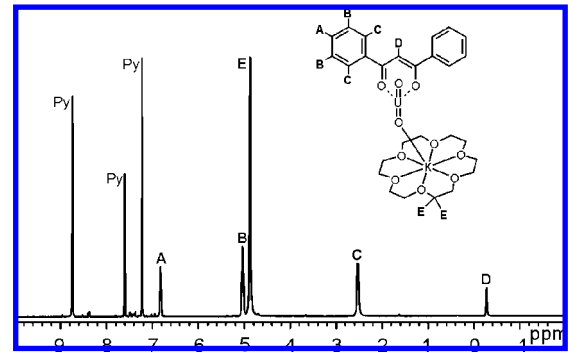

Figure 9. ^{1}H NMR spectrum at 400 MHz and at 298 K of **4** in a 7.2 mM pyridine solution.

resulting in the complete disruption of the tetrameric structure. However the disruption of the $K^+\cdots UO_2^+$ interaction could also play an important role.

To further evaluate the influence of the coordinated potassium ion on the solution structure and on the presence of CCI in solution, increasing amounts of (18C6) were added to a 14.9 mM pyridine solution of **2** (Figure S14, Supporting Information). The proton NMR spectra at increasing (18C6):K ratios show the successive increase of the signals assigned to the tetrameric species $[UO_2(dbm)_2]_4[\mu\text{-}K_4(Py)_x]$ and of those assigned to complex **4** accompanied by a decrease of the signals assigned to the tetrameric $\{[UO_2(dbm)_2]_4[\mu\text{-}K_6(Py)_x]\}^{2+}$ complex. At a (18C6):K ratio of 1:1 only the signals of complex **4** are observed.

The ^{1}H NMR spectrum of **4** in pyridine-d_5 (Figure 9) shows a single set of signals for the dbm protons, indicating the presence of $C2v$ symmetric species in solution. The PFGSTE diffusion NMR allowed calculation of an average molecular weight (M = 1010 g mol^{-1}) intermediate between the molecular weight of a monomeric and a dimeric species. This value is also intermediate between the molecular weight of monomeric species complexed or not by (18C6). In this case the assignment

Scheme 2

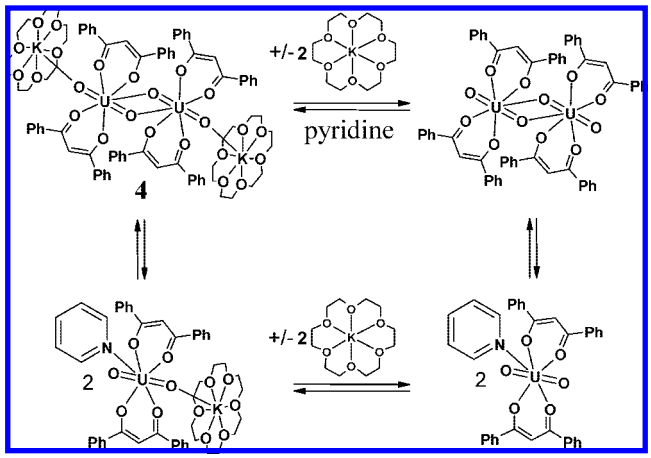

of the solution species remains ambiguous and could involve any or all of the equilibriums described in Scheme 2.

The ESI-MS mass spectroscopy shows only the molecular peak corresponding to $\{[UO_2(dbm)_2][K(18C6)]_2\}^+$ (m/z = 1322). The UV−vis spectrum of **4** in pyridine is very similar to the spectrum of **2** in dmso and differs significantly from those of the tetrameric complex in pyridine or thf (see Figures S1 and S2, Supporting Information). These results seem to indicate that monomeric species are predominant in solutions of **4** in pyridine, although $UO_2^+\cdots UO_2^+$ interaction can occur.

These results can be interpreted in terms of a lower affinity of the $[K(18C6)]^+$ cation, with respect to uncomplexed K^+, for the UO_2^+ oxygen atoms which leads to a reduced number of coordinated potassium ions in the presence of (18C6). Although the $UO_2^+\cdots UO_2^+$ interaction can still occur in the presence of (18C6) as evidenced by the isolation of the dimer **4** in the solid state, the partial removal of coordinated potassium ion leads to less strong CCIs in pyridine solution. Proton NMR studies show that the addition of potassium iodide (1.8 equiv) to a solution of **4** in pyridine leads again to formation of the tetrametallic complexes. This result provides additional compelling evidence that the potassium ion stabilizes the tetrameric versus the dimeric/monomeric forms. The effects of potassium on the formation of $UO_2^+\cdots UO_2^+$ interactions are probably of both structural and electronic nature. Potassium binding to the UO_2^+ oxygens not involved in CCI increases the Lewis acidity and therefore the electrophilic character of the U center, favoring the binding of a uranyl(V) oxygen in a $UO_2^+\cdots UO_2^+$ CCI. The weaker interaction of the potassium ions with the uranyl(V) oxygens involved in the CCI should have a minimal effect on the basicity of the uranyl oxygens and therefore on their ability to act as ligands in CCI. In contrast potassium binding to the dbm$^-$ oxygen atoms already bound to the uranyl(V) moiety also contributes to increase the Lewis acidity of the uranium center by decreasing the basicity of the ligand. Accordingly the multiple binding of potassium to the uranyl(V) and dbm$^-$ oxygen is probably crucial to the stability of the final tetrameric cation−cation assembly.

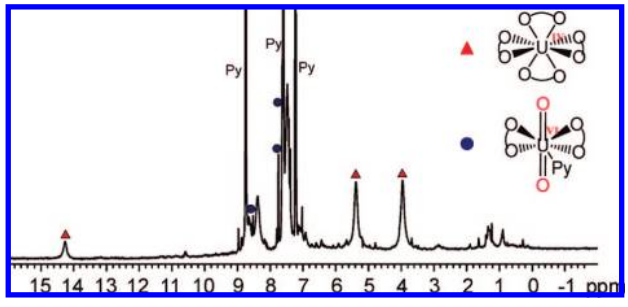

Figure 10. ^{1}H NMR spectrum at 400 MHz and 298 K of **2** in pyridine-d_5 after 7 days.

Stability Studies. CCIs have been proposed to play an important role in the disproportionation of the UO_2^+ into U(IV) and UO_2^{2+}.[11,12] In the previous section we have shown that only rigid tetrameric CCI complexes are present in thf solution, while partial or complete dissociation occurs to yield monomeric species in pyridine and in dmso, respectively. Dissociation of the tetrameric complexes is also observed on the NMR time scale in pyridine in the presence of (18C6), although $UO_2^+\cdots UO_2^+$ interactions can clearly occur under these conditions. In order to assess the effect of CCIs on the stability of these pentavalent uranyl species, stability studies were performed by proton NMR spectroscopy under different conditions.

The proton NMR spectra of pyridine solutions of complex **2** were recorded at different times (0−7 days) (Figure 10). Decomposition starts after a few hours and is complete after 7 days. The presence of the disproportionation product $[U(dbm)_4]$ was unambiguously characterized by NMR and by X-ray diffraction on isolated crystals. This product accounts for around 25% of the starting amount of UO_2^+ complex. The other identified species is $[UO_2(dbm)_2]$ (∼10%). Additional signals corresponding to dbm protons of unidentified species are found in the diamagnetic region. The isolated complex **3** has a very similar behavior in pyridine solution (Scheme 3).

The proton NMR of thf solutions of complex **3** were also recorded at different times (0−25 days; Figure S15, Supporting Information). The decomposition proceeds similarly to what is observed for **2** and **3** in pyridine, but is slower. It starts after ∼20 h, but 30% of the starting compound is still present after 7 days and decomposition is complete only after 25 days. The presence of the disproportionation product $[U(dbm)_4]$ was unambiguously characterized. This product accounts for ∼30% of the starting amount of UO_2^+ complex. The other identified species include some Kdbm and $[UO_2(dbm)_2]$ (∼15%). Addition of $[UO_2(dbm)_2]$ to the decomposed mixture allowed identification of the presence of the $[UO_2(dbm)_2]$ species as a decomposition product and led to a significant change in the signals of the $[U(dbm)_4]$ complex, which become narrower. This suggests the presence of an exchange interaction between the decomposition products.

Addition of water to the solution of **3** in thf results in a much faster decomposition with the total disappearance of the NMR signals assigned to the UO_2^{2+} species observed after 20 h. In this case, the decomposition also results in the formation of $[U(dbm)_4]$ (∼30% of the starting UO_2^+ after 20 h) (Scheme 4). Faster decomposition in the presence of water is in agreement with the disproportionation mechanism proposed by quantum chemical studies, which involves a protonation step of the bridging "yl" oxygen of the uranyl(V) cation−cation complex by water.[13]

The proton NMR of the complex **4** in pyridine at different times shows a somewhat different behavior. Decomposition also starts after ∼20 h and ∼40% of the starting compound is decomposed after 3 days, but afterward the decomposition process slows down and after 2 weeks ∼45% of the starting $[UO_2^V(dbm)_2]^-$ complex is still present (Scheme 5).

Furthermore the most important identified decomposition product is the potassium salt of the free dbm$^-$ ligand with only

Scheme 3

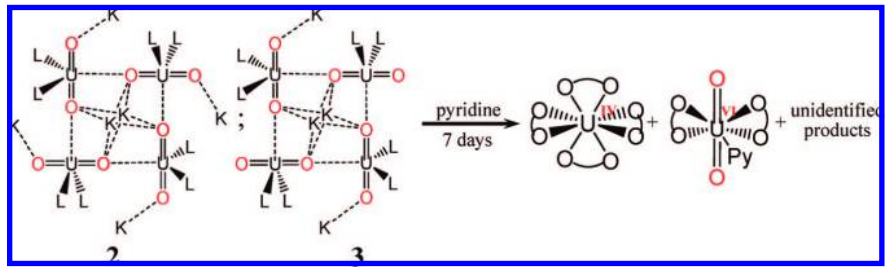

Scheme 4

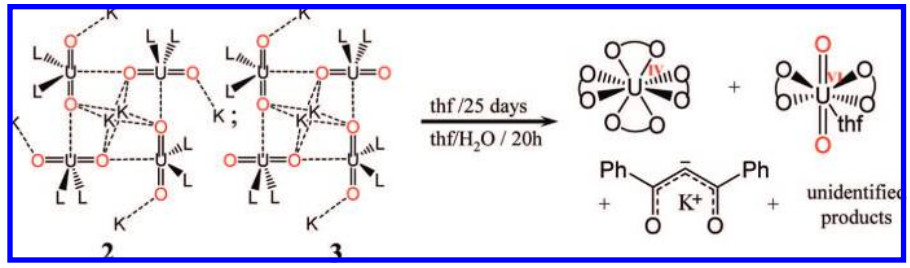

Scheme 5

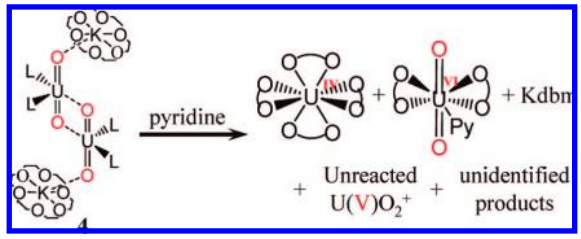

Scheme 6

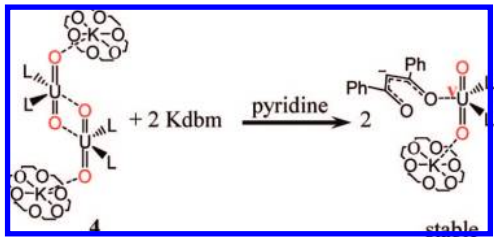

very small amounts of $[U(dbm)_4]$ formed after 7 days (7% of initial $[UO_2^V(dbm)_2]^-$ complex).

This suggests that the decomposition process proceeds according to a different mechanism with respect to the tetrameric species **2** and **3**, which probably involves ligand loss from a dimeric cation−cation intermediate associated with the electron-transfer process. The interaction of the resulting dbm^- with unreacted $[UO_2^V(dbm)_2]^-$ leads to its stabilization and is responsible for slowing down the decomposition process. This was confirmed by the high stability of a 1:1 solution of **4** and [K(18C6)(dbm)] in pyridine, for which no traces of decomposition were observed after several weeks (Scheme 6).

^{1}H 2D NOESY spectroscopy confirmed the presence of a rapid exchange between **4** and [K(18C6)(dbm)] in pyridine. The interaction of [K(18C6)(dbm)] with $[UO_2^V(dbm)_2]^-$ probably competes with the CCI preventing disproportionation. While the presence of the signals corresponding to hexavalent uranyl could not be identified in the spectrum of final decomposition products, the proton NMR spectra of **4** at different times shows an increasing broadening of the signals of the pentavalent uranyl species, suggesting its involvement in an exchange with the decomposition products. Addition of an excess of the $[UO_2^{VI}(dbm)_2]$ complex to the final mixture of disproportionation products leads to an important broadening of the signals of $[UO_2^V(dbm)_2]^-$ and of $[UO_2^{VI}(dbm)_2]$, in agreement with the presence of $[UO_2^{VI}(dbm)_2]$ among the decomposition products (Figure 11).

As discussed in the previous section, the complexes **2**, **3**, and **4** dissociate completely in dmso to yield the monomeric complexes $[UO_2(dbm)_2(dmso)_x]K$ or $[UO_2(dbm)_2(dmso)_x]K(18C6)$, which are fully stable (Schemes 7 and 8). The proton NMR shows no decomposition up to 1 month. The addition of 1000 equiv of H_2O to a dmso solution of $[UO_2(dbm)_2(dmso)_x]K$ results after 2 days in the presence of very small amounts of disproportionation products (3% U(IV) and 3% U(VI), showing that the presence of water promotes to some extent the disproportionation. The high stability of the monomeric pentavalent uranyl complex of dbm^- in dmso can be interpreted in terms of its strong coordination to the uranium center. The dmso coordination probably prevents the $UO_2^+\cdots UO_2^+$ interaction by competing with the uranyl(V) oxygen for the available binding site in the equatorial plane of the uranyl(V) moiety. While the retention of a rigid polymetallic arrangement in pyridine leads to complete decomposition of complexes **2** and **3**, the monomeric $[UO_2(dbm)_2(dmso)_x]K$ is fully stable. The observed stability of $[UO_2(dbm)_2(dmso)_x]K$ is in agreement with the electrochemical studies of Ikeda and co-workers, who observed that $[UO_2^{VI}(dbm)_2(dmso)]$ can be quasi-reversibly reduced in dmso to a stable and pure $[UO_2(dbm)_2(dmso)]K$ complex without any successive reaction.[22] The UV−vis solution spectrum of **2** in DMSO (Figure S2) is comparable to the one reported by Ikeda[22] for the electrochemically generated $[UO_2(dbm)_2(dmso)]^-$ complex, while a significantly different shape is found for the UV−vis solution spectrum of **2** and **3** in pyridine (Figure S1, Supporting Information). The presence of CCI is probably responsible for the observed differences, but the transitions due to CCI are difficult to trace.

In conclusion, these results provide strong evidence that the formation of inner-sphere CC ($UO_2^+\cdots UO_2^+$) complexes is

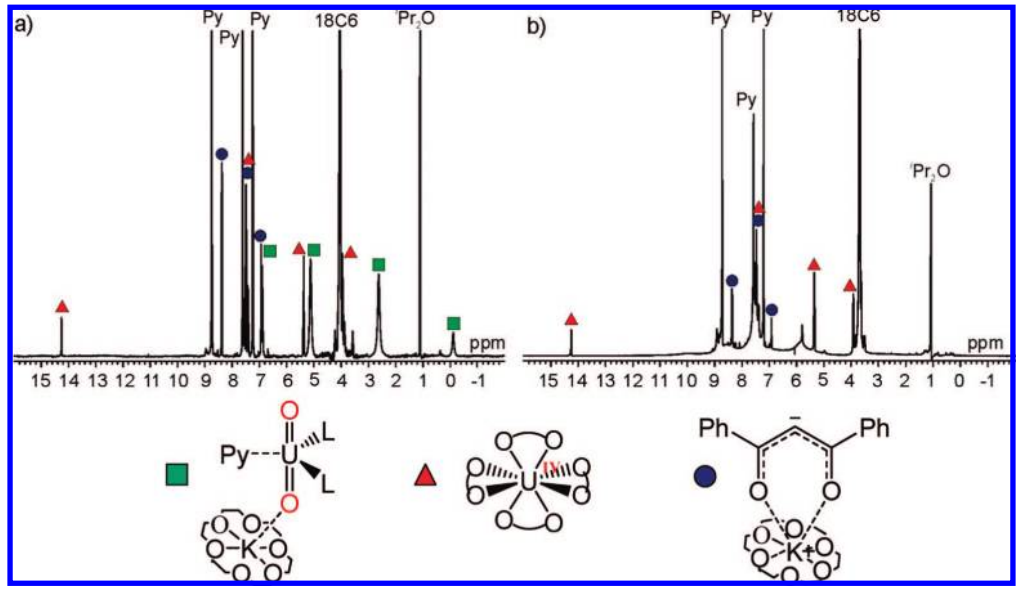

Figure 11. ^{1}H NMR spectra of a 7.2 mM solution of **4** in pyridine-d_5 at 400 MHz and 298 K (a) after 28 days and (b) after 28 days and addition of $[UO_2(dbm)_2Py]$ (signals for dbm protons of $[UO_2(dbm)_2K(18C6)]_2$ (green squares); [Kdbm(18C6)] (blue dots); $[U(dbm)_4]$ (red triangles)).

Scheme 7

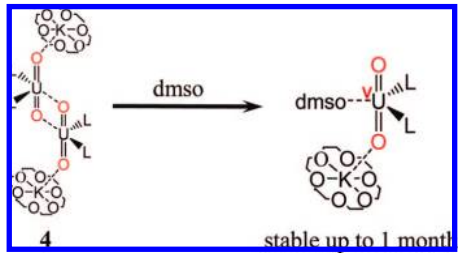

Scheme 8

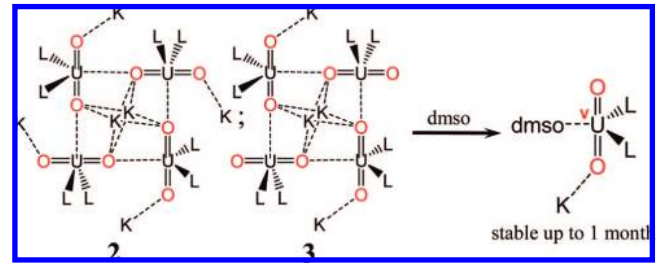

involved in the dispropotionation of pentavalent uranyl in organic solvents. Furthermore we have showed that counterion binding can stabilize the $UO_2^+\cdots UO_2^+$ interaction, resulting in fast decomposition. Conditions such as the presence of coordinating solvent or anions that prevent the formation of CCI complexes in solution stop the decomposition of pentavalent uranyl.

Both electronic and steric factors probably contribute to the instability of the complexes of pentavalent uranyl. Preliminary studies on diketonate ligands presenting groups with different steric hindrance show that decomposition occurs rapidly in all cases in pyridine or thf with these bidentate ligands, but the bulkier groups lead to faster disproportionation rates. Bidentate ligands are well suited to isolate polymetallic intermediates, but a subtle balance of the steric hindrances minimizing ligand displacement and providing sufficient stability to cation−cation intermediates is crucial for the isolation of CC complexes.

These results also suggest that the stabilization of mononuclear pentavalent uranyl complexes suitable for reactivity studies could prove difficult with bidentate ligands and that ligands with higher denticity are likely to provide more stable species.

Magnetic Susceptibility. The rich magnetic properties of 5f elements make them very attractive for the design of actinide-based functional materials. However, the fundamental understanding of the molecular parameters governing magnetic exchange interactions and electron delocalization in molecular compounds of actinides remain very limited.[2,42,43] The $5f^1$ ions are particularly interesting for the interpretation of magnetic data because electron repulsion is absent. However the scarcity of reported U(V) complexes has also limited the number of magnetic studies on this oxidation state,[44−46] and only one example of unambiguous antiferromagnetic coupling between two U(V) ions covalently linked by bridging imido ligands has been described.[35] Temperature-dependent magnetic susceptibility data were collected for the isolated analytically pure microcrystalline **1**, **3**, and **4** from 2 to 300 K and are shown in Figures 12 and 13, respectively. Samples of **1** display effective magnetic moments that vary with the temperature, reaching an effective magnetic moment of 2.57 μ_B per uranium at 300 K, which is very close to the theoretical value calculated for the free $5f^1$ ion in the L-S coupling scheme ($\mu_{eff} = 2.54\ \mu_B$)[47] thus suggesting the presence of well localized 5f electrons. The plot of the magnetic χ and χT data versus T of **1** (Figure 12) show

(42) Clark, D. L.; Hecker, S. S.; Jarvinen, G. D.; Neu, M. P. *The Chemistry of the Actinide and Transactinide Elements*; Springer: Dordrecht, 2006.
(43) Schelter, E. J.; Morris, D. E.; Scott, B. L.; Thompson, J. D.; Kiplinger, J. L. *Inorg. Chem.* **2007**, *46*, 5528–5536.
(44) Selbin, J.; Ortego, J. D. *Chem. Rev.* **1969**, *69*, 657–671.
(45) Graves, C. R.; Yang, P.; Kozimor, S. A.; Vaughn, A. E.; Clark, D. L.; Conradson, S. D.; Schelter, E. J.; Scott, B. L.; Thompson, J. D.; Hay, P. J.; Morris, D. E.; Kiplinger, J. L. *J. Am. Chem. Soc.* **2008**, *130*, 5272–5285.
(46) Castro-Rodriguez, I.; Olsen, K.; Gantzel, P.; Meyer, K. *J. Am. Chem. Soc.* **2003**, *125*, 4565–4571.
(47) Boudreaux, E. A.; Mulay, L. N. *Theory and Applications of Molecular Paramagnetism*; Wiley: New York, 1976; p 512.

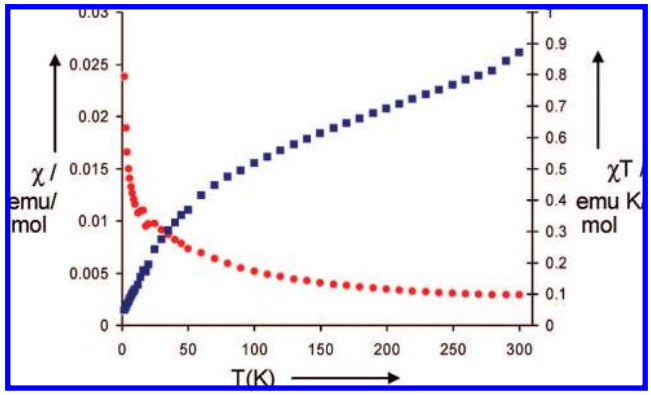

Figure 12. Temperature-dependent magnetic susceptibility data for **1** in the range of 2−300 K. At 300 K we calculated a μ_{eff} of 2.57 μ_B per uranium ($\chi_{dia} = -5.34 \times 10^{-4}$ emu mol^{-1}, $m = 31.41$ mg, $M = 1116.63$ g mol^{-1}).

two distinct temperature regions with different slopes: a high temperature regime between 50 and 300 K, which is linear with a large slope, and a lower temperature regime between 2 and ∼50K where the χT product decreases rapidly. Such temperature dependency has been observed in a few isolated imido complexes of U(V) and has been interpreted in terms of the presence of an isolated crystal field ground state (only contribution to the magnetization at low temperature) and of an excited crystal field state that becomes populated at high temperatures, therefore contributing to the magnetization.[2,35,45] The temperature dependency plots of χ and χT of both polymetallic complexes **3** and **4** show a similar behavior in the high temperature region, but they reach an effective magnetic moment per uranium at 300 K ($\mu_{eff} = 1.64$ μ_B for **3** and $\mu_{eff} = 1.69$ μ_B for **4**), much lower than the one found for **1** and the theoretical value calculated for the free $5f^1$ ion. Similar low values of the effective magnetic moment at high temperature have been reported for simple coordination complexes of the halides,[44] for mononuclear imido complexes,[2] and for polyoxoclusters of U(V) with a U_6O_{13} core.[48]

The presence of an antiferromagnetic coupling at room temperature was proposed to explain the low effective magnetic moment in this polyoxocluster (1.8 μ_B), while the low magnetic moment observed in mononuclear compounds has been interpreted in terms of a covalent character of the metal−ligand interaction that results in a reduction of the orbital magnetism,[46] although this interpretation appears controversial.[45]To elucidate if the low effective magnetic moment of the tetranuclear complex **3** and of the dinuclear complex **4** could arise from antiferromagnetic interactions at room temperature, we have compared the magnetic moment measured in the solid state with the one measured in solution by the Evans method.[49] The value of the magnetic moment of **3** measured in pyridine solution (1.6 μ_B at 298 K) where it retains its polynuclear structure is very similar to the value found in the solid state and to the value measured in dmso solution where the complex is monomeric (1.7 μ_B). A similar value was measured for complex **4** in pyridine solution (1.5 μ_B). These results rule out the presence of an antiferromagnetic coupling in complexes **3** and **4** at room temperature. In the context of the very limited literature on

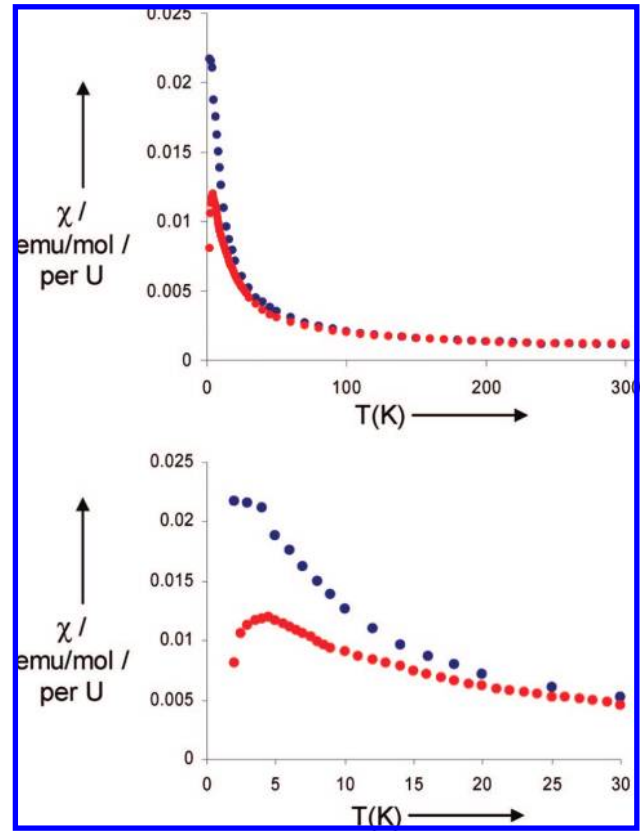

Figure 13. Temperature-dependent magnetic susceptibility data for **3** (blue circles) and **4** (red circles) in the range of 2−300 K. A μ_{eff} of 1.64 μ_B per uranium at 300 K was calculated for **3** ($\chi_{dia} = -1.53 \times 10^{-3}$ emu mol^{-1}, $m = 5.80$ mg, $M = 3220.82$ g mol^{-1}). A μ_{eff} of 1.69 μ_B per uranium at 300 K was calculated for **4** ($\chi_{dia} = -9.33 \times 10^{-4}$ emu mol^{-1}, $m = 15.00$ mg, $M = 2039.52$ g mol^{-1}).

magnetic studies of uranium(V) compounds, a possible interpretation of the reduced magnetic moment measured at room temperature for **3** and **4** could be the presence of a covalent contribution to the metal−ligand interaction in complexes **3** and **4**. However a recent report on a series of analogous imido halide complexes of U(V) show that simple conclusions on the extent of covalency are difficult to draw from room temperature magnetic moments.[45]

The magnetic behavior of **4** at very low temperature differs significantly from the behavior observed for **1** and shows unambiguously the presence of antiferromagnetic coupling between the two oxo-bridged U(V) ions (Figure 13) with the appearance of a maximum in χ versus T at ∼5 K. Magnetic coupling is likely to occur through a superexchange pathway mediated by the uranyl(V) oxygens involved in the diamond-shaped CCI. Magnetic studies on neptunyl frameworks have shown that CCIs (resulting in Np−Np distance of about 4.1 Å) can provide a superexchange pathway that leads to magnetic ordering.[8] While the maximum in χ versus T appeared at higher temperature (∼20 K) in the only other example of reported $5f^1-5f^1$ magnetic coupling,[35] this is the first example of magnetic coupling between uranium ions mediated by oxo ligands in an isolated molecule. The χT data versus T of **3** show two different regimes with a breaking point at 25K as observed for **4**. In **3** however, the χ data increase with decreasing the temperature until 4 K, where the magnetic susceptibility probably achieves a maximum. However, the lack of information at lower temperatures makes it difficult to ascertain if magnetic

(48) Duval, P. B.; Burns, C. J.; Clark, D. L.; Morris, D. E.; Scott, B. L.; Thompson, J. D.; Werkema, E. L.; Jia, L.; Andersen, R. A. *Angew. Chem., Int. Ed.* **2001**, *40*, 3357–3361.
(49) Evans, D. F. *J. Am. Chem. Soc.* **1959**, 2003–2005.

coupling occurs for the tetrameric complex **3** with a maximum at lower temperature than for complex **4**. The complex shows a linear field dependence of the magnetization at 6 K.

The different behavior of complexes **3** and **4** can be related to the very different geometric arrangement of the interacting UO_2^+ groups (see Figure 4), which also leads to significantly shorter U−U distance in complex **4** (3.462 Å in **4** vs 4.318(6) Å average U−U distance in **3**). These results suggest that CCI complexes could prove particularly well suited for establishing a magnetostructural correlation in uranium chemistry.

Extensive studies have been performed on oxo-bridged d-block metal complexes in order to establish magnetostructural correlations.[50] A fit to experimental data for a large number of oxide-bridged diiron(III) complexes indicated that the magnetic interaction decreases when M−O distance increases or when the Fe−O−Fe angle increases.[51] However magnetostructural correlations between complexes of different nuclearity is less straightforward even for these extensively studied systems.[52]

Conclusions

We have described synthetic procedures that allow for the isolation of cation−cation complexes of pentavalent uranyl. The structural characterization of these new cation−cation complexes, tetrameric and dimeric, of pentavalent uranyl with the dbm^- ligand, has allowed the unambiguous identification of the presence of $UO_2^+\cdots UO_2^+$ CCIs in solution. Furthermore the presented results highlight the importance of the presence of a cation binding the uranyl(V) oxygen ($K^+\cdots UO_2^+$ CCIs) in the stabilization of these interactions. NMR studies have been used for the first time to unambiguously identify CCIs in solution and to relate the stability of pentavalent uranyl with the formation of cation−cation complexes. The decomposition of pentavalent uranyl was not observed in conditions that block CCIs, whereas fast disproportionation of pentavalent uranyl to form U(IV) and U(VI) species and other unidentified products is observed for cation−cation complexes. The presence of coordinating solvents or anions can prevent the CCIs by competing with the "yl" oxygen in the coordination of the uranium center, showing that an appropriately chosen ligand set can lead to highly stable UO_2^+ complex. The presence of water was found to accelerate significantly the decomposition when CCIs could be formed, while a smaller effect is observed on monomeric species, supporting the importance of CCIs in the disproportionation of pentavalent uranyl in water.

Despite their low solution stability, an appropriate choice of synthetic conditions allows the isolation of the tetrameric $\{[UO_2(dbm)_2]_2[\mu\text{-}K(MeCN)_2][\mu_8\text{-}K]\}_2$ and the dimeric $[UO_2(dbm)_2K(18C6)]_2$ in a pure form, making possible the study of their magnetic properties. The measured temperature-dependent magnetic susceptibility highlights the presence of unambiguous antiferromagnetic coupling between the two uranium centers of the $[UO_2(dbm)_2K(18C6)]_2$ dimer with appearance of a maximum in χ versus T at ~5 K. The coupling probably occurs via a superexchange pathway through the bridging oxygen atoms involved in the diamond-shaped CCI. The different behavior of the tetrameric complex, which probably involves a magnetic coupling occurring at lower temperature, can be ascribed to the different geometric arrangement of the interacting uranyl(V) groups (T-shaped in the tetramer versus diamond-shaped in the dimer). These results provide the first example of magnetic coupling between uranium ions via uranyl(V) oxo bridges and open broad perspectives for the use of cation−cation complexes as a new class of polymetallic uranium compounds for the study of magnetic interactions and intermetallic communication in actinides and for the development of new functional actinides materials. Work in both directions is in progress.

Experimental Section

General. All manipulations were carried out under an inert argon atmosphere using Schlenk techniques and a MBraun glovebox equipped with a purifier unit. The water and oxygen levels were always kept at less than 1 ppm. The solvents were purchased from Aldrich in their anhydrous form, conditioned under argon, and vacuum-distilled from K/benzophenone (pyridine, thf, hexane, and diisopropylether) or CaH_2 (acetonitrile). Commercial anhydrous dmso-d_6 was further dried over molecular sieves preliminarily heated at 200°. Depleted uranium turnings were purchased from the "Société Industrielle du Combustible Nucléaire" of Annecy (France). Dibenzoylmethane (dbmH), pyridine *N*-oxide, and 18-crown-6 (18C6) were purchased from Aldrich and dried under vacuum at 50 °C for 7 days. $[UI_3(thf)_4]$[53] and $[UI_4(PhCN)_4]$[54] were synthesized as previously described. Elemental analyses were performed under argon by Analytische Laboratorien GMBH at Lindlar, Germany.

$[UO_2(dbm)_2Py]$ was synthesized as previously described.[55] ^{1}H NMR (pyridine-d_5, 298 K, 400 MHz): 8.64 (s, 8H); 7.63 (s, 12H); 7.37 (s, 2H). ^{1}H NMR (thf-d_8, 298 K, 400 MHz): 8.57 (s, 8H); 7.62 (s, 12H); 7.40 (s, 2H). $[U(dbm)_4]$[56] was prepared in situ by reacting 1 equiv of $[UI_4(PhCN)_4]$ and 4 equiv of Kdbm, ^{1}H NMR $[U(dbm)_4]$ (thf-d_8, 298 K, 400 MHz): 14.17 (s, 4H); 7.50 (s, 8H); 4.97 (s, 16H); 2.56(s, 16H). ^{1}H NMR $[U(dbm)_4]$: (pyridine-d_5, 298 K, 400 MHz): 14.25 (s, 4H); 7.59 (s, 8H); 5.37 (s, 16H); 3.95(s, 16H). ^{1}H NMR $[U(dbm)_4]$: (dmso-d_6, 298 K, 400 MHz): 15.54 (s, 4H); 6.23 (s, 8H); 5.81 (s, 16H); 4.86(s, 16H).

FTIR spectra were recorded with a Perkin-Elmer 1600 Series FTIR spectrophotometer. UV−vis measurements were carried out with a Varian Cary 50 Probe spectrophotometer in quartz cells (optical path lengths: 1 mm and 1 cm) adapted with J. Young valves. ^{1}H NMR spectra were recorded on Varian UNITY and MERCURY 400 MHz and Bruker 200 MHz spectrometers. NMR chemical shifts are reported in ppm with solvent as internal reference.

Static magnetic properties were measured using a Quantum Design SQUID MPMS-XL 5.0 susceptometer; ultra-low field capability ±0.05 G for the 5 T magnets; continuous low temperature control/temperature sweep mode (CLTC), sweep rate 0.001−10 K/min.

The samples were pressed under argon into a Kel-F or an aluminum container, which was then sealed under vacuum in a 5 mm Suprasil quartz tube. Contribution to the magnetization from the Kel-F or the aluminum container and tube were measured independently and subtracted from the total measured signal. Diamagnetic corrections were made using Pascal's constants.

Mass spectra were obtained with a Finnigan LCQ-ion trap equipped with an electrospray source in a 1:5 pyridine/acetonitrile mixture that was prepared and filtered on microporous filters in the glovebox and maintained under argon until injection in the spectrometer. The experimental isotopic profile was compared in each case to the theoretical one (see Supporting Information).

(50) Kahn, O. *Molecular Magnetism*; Wiley-WCH: New York, 1993.
(51) Weihe, H.; Gudel, H. U. *J. Am. Chem. Soc.* **1997**, *119*, 6539–6543.
(52) Canada-Vilalta, C.; O'Brien, T. A.; Brechin, E. K.; Pink, M.; Davidson, E. R.; Christou, G. *Inorg. Chem.* **2004**, *43*, 5505–5521.
(53) Avens, L. R.; Bott, S. G.; Clark, D. L.; Sattelberger, A. P.; Watkin, J. G.; Zwick, B. D. *Inorg. Chem.* **1994**, *33*, 2248–2256.
(54) Enriquez, A. E.; Scott, B. L.; Neu, M. P. *Inorg. Chem.* **2005**, *44*, 7403–7413.
(55) Alcock, N. W.; Flanders, D. J.; Pennington, M.; Brown, D. *Acta Crystallogr., Sect. C: Cryst. Struct. Commun.* **1987**, *43*, 1476–1480.
(56) Kepert, D. L.; Patrick, J. M.; White, A. H. *J. Chem. Soc., Dalton Trans.* **1983**, 567–570.

Synthesis of Kdbm. A solution of dbmH (200 mg, 0.89 mmol, 1 equiv) in thf (3 mL) was added to a suspension of KH (39.2 mg, 0.98 mmol, 1.1 equiv) in thf (1 mL). The mixture was stirred for 1 h until the gas clearing was complete, resulting in a yellow solution. After removal of the excess of KH by filtration, 4 mL of diisopropylether was slowly added to the resulting pale yellow filtrate. The Kdbm was precipitated out of the solution as a pale yellow solid, which was filtered, washed with a small amount of thf, and dried under vacuum (208 mg, 88% yield). ^{1}H NMR (pyridine-d_5, 298 K, 400 MHz): 8.64 (m, 6H, $H_{para,meta}$-Ph); 7.62 (m, 4H, H_{ortho}-Ph); 7.34 (s, 1H, CO-CH-CO). ^{1}H NMR (dmso-d_6, 298 K, 200 MHz): 7.79 (m, 4H, H_{ortho}-Ph); 7.32 (m, 6H, $H_{para,meta}$-Ph); 6.20 (s, 1H, CO-CH-CO). ^{1}H NMR (pyridine-d_5 + (18C6) (1equiv), 298 K, 400 MHz): 8.37 (d, J = 6.4 Hz, 4H, H_{ortho}-Ph); 7,48 (t, J = 6.4 Hz, 4H, H_{meta}-Ph); 7,39 (t, J = 6.4 Hz, 2H, H_{para}-Ph); 6.93 (s, 1H, CO-CH-CO).

Syntheses of Pentavalent Uranyl Complexes. The synthesis of $\{[UO_2Py_5][\mu\text{-}KI_2Py_2]\}_n$ (**1**) was performed in a gram scale according to the previously described procedure.[28] The higher scale and the use of a longer crystallization time (3 weeks) led to a significant increase of the final yield (75%). The synthesis of $\{[UO_2(dbm)_2]_2[\mu\text{-}K(Py)_2]_2[\mu_8\text{-}K(Py)]\}_2I_2\cdot Py_2$ (**2**) was performed on a 50 mg scale according to the previously described procedure (70% yield).[29] Anal. Calcd for $\{[UO_2(dbm)_2]_2[\mu\text{-}K(Py)_2]_2[\mu_8\text{-}K(Py)\}_2I_2\cdot Py_2\cdot 4^iPr_2O\cdot 4KI$: C 41.98, H 3.52, N 2.52. Found: C 42.15, H 3.70, N 2.62.

Synthesis of $\{[UO_2(dbm)_2]_2[\mu\text{-}K(MeCN)_2][\mu_8\text{-}K]\}_2$ (3). An acetonitrile suspension (0.4 mL) of Kdbm (40.2 mg, 153 μmol, 2 equiv) was added to an acetonitrile (0.4 mL) suspension of **1** (85.7 mg, 76.7 μmol, 1 equiv). A deep green solution was formed, which was then stirred for 15 min and filtered to remove a white solid. The deep green filtrate was allowed to stand at room temperature for 10 h to allow crystallization. Small blue crystals were obtained, filtered, washed with acetonitrile (0.5 mL), and dried (9.8 mg). The evaporation of the resulting filtrate allowed the isolation, after standing 24 h at room temperature, of a second crop of crystals, which were thoroughly washed with acetonitrile (2 mL) to remove traces of decomposition product ([U(dbm)$_4$]); 15.4 mg of analytically pure compound was obtained (total yield 42%). ^{1}H NMR (pyridine-d_5, 400 MHz, 298 K): δ 7.46 (t, J = 7.8 Hz, 8H); 6.40 (t, J = 7.0 Hz, 16H); 6.16 (t, J = 7.5 Hz, 8H); 5.66 (d, J = 7.0 Hz, 16H); 4.89 (t, J = 6.9 Hz, 16H); 3.60 (d, J = 6.5 Hz, 16H); 3.60 (s, 4H). ^{1}H NMR (thf-d_8, 400 MHz, 298 K): δ 7.38 (s, 8H); 6.35 (s, 16H); 6.02 (s, 8H); 5.31 (s, 16H); 4.56 (s, 16H); 2.87 (s, 16H); 1.95 (s, 4H). ^{1}H NMR (CD_3CN, 400 MHz, 298 K): δ 7.47 (s, 8H); 7.01 (s, 16H); 6.13 (s, 16H); 5.95 (s, 8H); 4.99 (s, 16H); 4.72 (s, 16H); 3.61 (s, 4H). ^{1}H NMR of **3** (thf-d_8, 323 K, 400 MHz): δ 7.32 (dd, J = 6.4, 8.6 Hz, 4H); 6.38 (dd, J = 6.4, 8.6 Hz, 8H); 6.02 ((dd, J = 6.4, 8.6 Hz, 4H); 5.38 (d, J = 8.6 Hz, 8H); 4.69 (dd, J = 6.4, 8.6 Hz, 8H); 3.19 (d, J = 6.4 Hz, 8H); 2.20 (s, 4H). ESI/MS m/z = 1549 $\{[UO_2(dbm)_2]_4K_6\}^{2+}$. Anal. Calcd for $\{[UO_2(dbm)_2]_2[\mu\text{-}K(MeCN)][\mu_8\text{-}K]\}_2$0.7KI: C 46.24, H2.94, N 0.87. Found: C 46.31, H 3.54, N 0.91.

Synthesis of $[UO_2(dbm)_2K(18C6)]_2$ (4). A solution of Kdbm (70.0 mg, 268 μmol, 2 equiv) in pyridine (2 mL) was added to a suspension (150 mg, 134 μmol, 1 eq U) of **1** in pyridine (1 mL). The mixture was stirred for 30 min until **1** completely dissolved to give a blue solution, which was subsequently filtered. The pyridine was removed under vacuum to give a blue solid, which was dissolved in thf (5 mL) to afford a blue solution and a white precipitate (KI). The precipitate was removed by filtration. A solution (1 mL) of 18-crown-6 (106.5 mg, 3 equiv) in thf was added to the filtrate, and the resulting solution was vigorously stirred for 30 s and then allowed to stand at room temperature for 15 min to afford a blue microcrystalline solid. The solid was filtered, washed three times with thf (3 mL) and dried under vacuum. Finally the solid was dissolved in pyridine (0.5 mL), and hexane (8 mL) was added to the resulting solution to yield **4** as a blue-green solid. The obtained blue-green solid was washed three times with hexane (3 mL) and dried under vacuum (61.6 mg, 45%) ESI/MS m/z = 1322 $\{[UO_2(dbm)_2][K(18C6)]_2\}^+$ Anal. Calcd for $C_{42}H_{46}UO_{12}K$: C, 49.46; H, 4.55; N, 0.00. Found: C, 49.32; H, 4.75; N, 0.33. ^{1}H NMR (pyridine-d_5, 298 K, 400 MHz): 6.82 (br, t. 4H, H_{para}-Ph); 5.03 (br dd, 8H, H_{meta}-Ph); 4.87 (br 24H, -CH_2O-); 2.52 (br D, 8H, H_{ortho}-Ph); −0.28 (br, 2H, CO-CH-CO). ^{1}H NMR of **4** (pyridine-d_5, 333 K, 400 MHz): 6.82 (br, 4H, H_{para}-Ph); 5.32 (br dd, 8H, H_{meta}-Ph); 4.76 (br 24H, -CH_2O-); 2.91 (br D, 8H, H_{ortho}-Ph); 0.32 (br, 2H, CO-CH-CO).

Stability Studies. The stability of **2** and **4** was examined in pyridine-d_5, and the stability of **3** and of a 1:1 mixture of **3** and water was studied in thf-d_8. In each case the concentration equalled 6.7 mM U. The samples were monitored in time by ^{1}H NMR at 400 MHz and 298 K. The NMR spectra were recorded after 80, 220, 460, 1560, 3000, 4400, 10080, 20160 min (for **4**), 80, 220, 460, 1560, 3000, 10080 min (for **2**), from 100 and 37500 min (for **3**) and from 10 to 1220 min for the 1:1 mixture of **3** with water. Amount (%) of each attributed species was estimated from integration and given in function of time (see Figures S15−S17, Supporting Information).

X-ray Crystallography. All diffraction data were taken using a Bruker SMART CCD area detector three-circle diffractometer (Mo Kα radiation, graphite monochromator, λ = 0.71073 Å). To prevent oxidation, the crystals were coated with a light hydrocarbon oil and quickly transferred to a stream of cold nitrogen on the diffractometer. The cell parameters were obtained with intensities detected on three batches of 15 frames with a 180 s and 10 s exposure time for, respectively, **3** and **4**. The crystal-detector distance was 5 cm. The data were collected for 0.3° increments in ω with a 120 s exposure time for **3** and 180 s for **4**. A full hemisphere of data was collected for each complex. At the end of data collection, the first 50 frames were recollected to establish that crystal decay had not taken place during the collection. Unique intensities with $I > 10\sigma(I)$ detected on all frames using the Bruker SMART program[57] were used to refine the values of the cell parameters. The substantial redundancy in data allows empirical absorption corrections to be applied using multiple measurements of equivalent reflections with the SADABS Bruker program.[57] Space groups were determined from systematic absences, and they were confirmed by the successful solution of the structure (Table 1). Complete information on crystal data and data collection parameters is given in Supporting Information. The structures were solved by direct methods using the SHELXTL 5.03 package.[58] For complexes **4**, all atoms, including hydrogen atoms, were found by difference Fourier syntheses. All non-hydrogen atoms were anisotropically refined on F^2, and hydrogen atoms were isotropically refined. For complexes **3** hydrogen atoms were included in calculated positions with isotropical thermal coefficients.

Acknowledgment. This work was supported by the Commissariat à l'Energie Atomique, Direction de l'Energie Nucléaire and by the "Actinet" European network. We thank Fabien Burdet for preliminary work, Pierre Alain Bayle for his help with the NMR experiments, Jean-François Jacquot for the magnetic measurements, and Colette LeBrun for the help with the ESI-MS experiments.

Supporting Information Available: Crystallographic details for compounds **3** and **4** as CIF files; UV−vis spectra of **2**, **3**, and **4**; NMR spectra and IR spectra of **2** and **3**; description of the pulse sequence, equations, and experimental conditions used for the determination of the diffusion coefficients. This material is available free of charge via the Internet at http://pubs.acs.org.

JA804766R

(57) *SMART: Software Package for Use with the SMART Diffractometer*; Bruker: Madison, WI, 1995.
(58) Sheldrick, G. M. *SHELXTL, 6.14*; University of Göttingen: Göttingen, Germany, 2006.